BIOCHEMISTRY
including biophysical chemistry & molecular biology

Article

Stability and Membrane Orientation of the Fukutin Transmembrane Domain: A Combined Multiscale Molecular Dynamics and Circular Dichroism Study

Daniel A Holdbrook, Yuk Ming Leung, Thomas J Piggot, Phedra Marius, Philip T.F. Williamson, and Syma Khalid

Biochemistry, **Just Accepted Manuscript** • DOI: 10.1021/bi101743w • Publication Date (Web): 24 November 2010

Just Accepted

Biochemistry is published by the American Chemical Society. 1155 Sixteenth Street N.W., Washington, DC 20036

Stability and Membrane Orientation of the Fukutin Transmembrane Domain: A Combined Multiscale Molecular Dynamics and Circular Dichroism Study

Daniel A. Holdbrook[1], Yuk Ming Leung[1], Thomas J. Piggot[1], Phedra Marius[2], Philip T.F. Williamson[2*] and Syma Khalid[1*]

[1]*School of Chemistry, University of Southampton, Highfield, Southampton, SO17 1BJ, UK*

[2]*School of Biological Sciences, University of Southampton, Highfield, Southampton SO17 1BJ, UK*

RECEIVED DATE (automatically inserted by publisher);

[*]To whom correspondence should be addressed at:

Email: P.T.Williamson@soton.ac.uk, Phone: +44 (0) 2380 594350

Email: S.Khalid@soton.ac.uk, Phone: +44(0) 2380 59476 Fax: +44 (0)23 8059 3781

TITLE RUNNING HEAD: Membrane orientation of a simple peptide.

PM and PTFW are funded by a Wellcome Trust Fellowship to PTFW. SK is an RCUK fellow. TJP is funded by BBSRC.

Abbreviations

Fukutin transmembrane domain: FK1TMD

Golgi apparatus: GA

Molecular dynamics: MD

Atomistic molecular dynamics: ATMD

Coarse-grained molecular dynamics: CGMD

Circular dichroism: CD

Cholesterol: CHOL

1,2-dipalmitoyl-sn-glycero-3-phoshpatidylinositol 4,5-bisphosphate: PIP2

1,2-dihexanoyl-sn-glycero-3-phosphocholine: DHPC

1,2-didecanoyl-sn-glycero-3-phosphocholine: DDPC

Dilauroyl-phosphatidylcholine: DLPC

Dimyristoyl-phosphatidylcholine: DMPC

Dipalmitoyl-phosphatidylcholine: DPPC

Palmitoyloleoyl-phosphatidylcholine: POPC

Palmitoyloleoyl phosphatidylserine: POPS

Phosphatidylethanolamine: PE

Phosphatidylserine: PS

Inositol 1,4,5-trisphosphate: IP3

Sphingomyelin: SM

Multilamellar vesicles: MLV

Small unilamellar vesicle: SUV

ABSTRACT: The N-terminal domain of Fukutin-I has been implicated in the localization of the protein in the endoplasmic reticulum/Golgi apparatus. It has been proposed to mediate this through its interaction with the thinner lipid bilayers found in these compartments. Here we have employed multi-scale molecular dynamics simulations and circular dichroism spectroscopy to explore the structure, stability and orientation of the short 36-residue N-terminal of Fukutin-I (FK1TMD) in lipids of differing tail lengths. Our results show that FK1TMD adopts a stable helical conformation in phosphatidylcholine lipids when orientated with its principal axis perpendicular to the bilayer plane. The stability of the helix is largely insensitive to the lipid tail length, avoiding hydrophobic mismatch by virtue of its mobility and ability to tilt within the lipid bilayers. This suggests that changes in FK1TMD tilt in response to bilayer properties may be implicated in the regulation of its trafficking. Coarse-grained simulations of the complex Golgi membrane suggest the N-terminal domain may induce the formation of microdomains in the surrounding membrane through its preferential interaction with 1,2-dipalmitoyl-sn-glycero-3-phoshpatidylinositol 4,5-bisphosphate (PIP2) lipids.

Recently, a number of genes have been identified which are implicated in the O-linked glycosylation of the α-dystroglycan (aDG), a vital component of the dystrophin associated complex that anchors muscle fibres to the extracellular scaffold (*1*). These genes include *fukutin-I (fk1)*, *fukutin related protein (FKRP), LARGE, POMGnT1, POMT1 and POMT2*. Mutations in these genes have been shown to lead to the aberrant glycosylation of the aDG resulting in a broad spectrum of congenital muscular dystrophies. Analysis of these genes suggests that they code for Type-II membrane proteins with putative glycosyltransferase activity, consistent with the hypoglycosylation of the aDG observed in patients carrying mutations in these genes (*1*). A number of studies have since demonstrated that these proteins are located in the ER/Golgi complex consistent with their proposed role in the glycosylation of the aDG (*2-5*). Interestingly a number of mutations identified in these genes result in the mislocalisation of the protein within the cell, suggesting that their retention within the ER/Golgi complex is vital for the appropriate glycosylation of aDG (*3*).

Protein retention within the ER/GA is a highly dynamic process which relies crucially on the regulation of both antero- and retro-grade transport steps (*6*). A number of bioinformatic and biochemical studies have demonstrated that retrograde transport is largely regulated by receptor mediated recognition of specific extra-membranous motifs on ER/Golgi resident proteins (*7*). In contrast anterograde transport appears to be dependent on the shorter transmembrane domain that is typically found in ER/Golgi resident proteins (*7, 8*). Indeed, studies of the N-terminal transmembrane domains of FK1 and FKRP have been shown to be sufficient to retain the protein within the GA(*9*). It has been suggested that the retention of ER/Golgi resident proteins may be mediated through the interaction of these shortened transmembrane domains and the distinctive lipid composition found in the ER/Golgi membranes. Although the role of the N-terminal TMDs in the retention of these proteins within the ER/Golgi apparatus is clear we are far from a molecular description of this process and currently several models based on lipid mediated protein sorting and protein oligomerisation have been proposed (*6, 8, 10, 11*).

To begin to investigate the role that the bilayer composition within the ER/GA may play on the retention of these proteins, we have undertaken a combined molecular dynamics (MD) and circular dichroism (CD) study of the transmembrane domain of the protein encoded by *fukutin* in a range of bilayer compositions in order to ascertain how the protein responds to differing bilayer thicknesses. We focus on FK1TMD, a short fragment composed of the first 36 N-terminal residues of Fukutin, which is thought to insert into the membrane of the Golgi apparatus. Whilst the structure of FK1TMD has not been resolved, preliminary CD studies indicated a mostly α-helical under conditions that mimic the lipid bilayer (*12*).

METHODS

Atomistic molecular dynamics (ATMD) simulations of FK1TMD (modeled as an idealized α-helix) in (i) water, (ii) 1M NaCl, (iii) a dimyristoyl-phosphatidylcholine (DMPC) bilayer and (iv) a dipalmitoyl-phosphatidylcholine (DPPC) bilayer. The insertion of FK1TMD into (i) dilauroyl-phosphatidylcholine (DLPC) (ii) DPPC, (iii) POPC, (iv) POPS, and (v) mixed lipid bilayers was studied *via* coarse-grained molecular dynamics (CGMD) simulations.

Generation of fukutin FK1TMD model. A model of the 36-residue transmembrane domain of fukutin (FK1TMD) was created by threading the FK1TMD sequence to an idealized α-helix using Modeller 9v7 (*13*). The resulting helix was evaluated for stereochemical integrity using Procheck (*14*). This model was used for all of the atomistic simulations and also for creating the coarse-grained version of the FK1TMD.

Details of atomistic simulations. Atomistic Simulations were performed using GROMACS 4.0.7 (**www.gromacs.org**) (*15-17*). The simulations used an extended united atom version of the GROMOS96 forcefield (*18*). Berger parameters were used for phospholipids, as described in (*19*). Water molecules were treated explicitly using the SPC water model (*20*). Sodium and chloride ions were used to neutralize the charge of the simulation systems. All lipid and protein bonds were constrained using the LINCS algorithm (*21*), and water molecules were constrained using the SETTLE algorithm (*22*), allowing for a time step of 2 fs to be used. The velocity rescaling thermostat, with a time constant

for the coupling of 0.1 ps, was used to maintain the system temperature (*23*). The Berendsen barostat, with a time constant of 1.0 ps, was used to maintain the system pressure at 1.0 bar (*24*). Electrostatic interactions used a cut-off of 1.0 nm with interactions beyond this cutoff treated using the smooth particle mesh Ewald (PME) method (*25*). The van der Waals interactions also used a cut off of 1.0 nm with a long-range dispersion correction applied for the energy and pressure. The neighbor list was updated every 10 steps. The system components of each simulation are summarized in supplementary table 1. All simulations were run for 50 ns. The conformational properties of FK1TMD were analyzed using GROMACS tools and the DSSP program (*26*). Visualization used VMD (*27*).

Details of coarse-grained simulations. All CG simulations were performed using GROMACS 4.0.7 (www.gromacs.org) (*15-17*) with the MARTINI CG force fields. All simulations involved self-assembly of a lipid bilayer in the presence of one FK1TMD molecule from a random configuration of protein, lipids, ions and water as described in (*28-30*). The CG parameters for DPPC, DLPC, POPC, ions and water molecules were as described as in (*28*). The parameters for the 1,2-dipalmitoyl-sn-glycero-3-phoshpatidylinositol 4,5-bisphosphate (PIP2) lipid headgroup were derived through matching the bond and angle distributions from a CG inositol 1,4,5-trisphosphate (IP3) (*31*) simulation to atomistic simulations of IP3 performed using the GROMOS carbohydrate parameters (*32*). The remainder of the PIP2 lipid parameters were the same as those used for the CG DPPC lipid. Parameters for amino acids were as described in (*29, 33, 34*). The integrity of the FK1TMD helix was retained by implementing an elastic network model as described in (*33*). For simulations of FK1TMD in the more complex Golgi apparatus membrane, we used the MARTINI2.0 forcefield due to the greater range of lipid models available (*35*). The complex GA membrane was composed of 50% PC, 20% phosphatidylethanolamine (PE), 12% PIP2, 8% phosphatidylserine (PS), and 10% sphingomyelin (SM). All phospholipids had palmitoyl fatty acid tails in both the sn1 and sn2 positions of the glycerol backbone. The ratio of phospholipid to cholesterol was 16:1 (0.16). This composition is similar to that of the GA (*36*). As with the atomistic simulations, analyses of the CG simulations were performed using GROMACS tools and locally written code and visualization used VMD (*27*).

Details of circular dichroism experiments. The hydrophobic peptide FK1TMD (MQRINKNVVL ALLTLTSSAF LLFQLYYYKH YLSARN) was synthesized by Peptide Protein Research Ltd, UK to more than 50% purity. The DHPC (C6:0), DDPC (C10:0), DLPC (C12:0), DMPC (C14:0), and DPPC (C16:0) were purchased from Avanti Polar Lipids, USA. Sodium phosphate was obtained from Sigma.

For lipids with chain lengths greater than 10 carbon atoms, FK1TMD peptide was reconstituted into unilamellar vesicles by dissolving peptide and lipid at a molar ratio of 100:1 in methanol. This was dried to a thin film by vacuum evaporation. Multilamellar vesicles (MLVs) were formed by hydration and agitation in 5 mM sodium phosphate buffer, pH 7.4. MLVs were sonicated to clarity to form small unilamellar vesicles (SUVs). The final concentration of FK1TMD in the CD samples was 0.2 mg mL^{-1} as determined by it absorbance at 280 nm (E_{280}=5960 M^{-1} cm^{-1}). For DHPC (C6:0) the samples were prepared in an identical manner resulting in the reconstitution of FK1TMD into DHPC micelles.

The CD spectrum of FK1TMD peptide reconstituted in unilamellar vesicles composed of saturated phospholipids of varying chain lengths was measured using a Jasco J720 spectropolarimeter fitted with a heater and a 1-mm- path-length quartz cuvette (Hellma) at 25°C and at 43°C. The spectrum scan was performed from 300 to 190 nm using a spectral bandwidth of 2 nm, scanning speed of 100 nm min^{-1} and 4 second response time. Six spectra were recorded and averaged for subsequent analysis. CD spectra were analyzed between 195 and 240 nm to determine the secondary structure composition of the FK1TMD in the different lipid environments using the CONTIN/LL analysis algorithm (*37, 38*) provided on the Dichroweb CD analysis server (*39, 40*). The analysis was performed using basis set 7 that has been widely used to study secondary structural elements of membrane peptides and surface associated proteins.

RESULTS

Atomistic simulations. Initially, the stability of the FK1TMD model was assessed in an aqueous environment. The protein lost much of its α-helical structure within the first 10 ns of simulation; by the end of the 50 ns simulation only residues V8 to L13 and L25 to H30 were in an α-helical conformation (see supplementary Figures 1 and 2).

Next, the stability of the FK1TMD model in the vicinity of a membrane-mimetic phospholipid bilayer was investigated. Simulations were initiated with the FK1TMD model in two positions relative to the phospholipid bilayer (i) in the water region just above the phospholipid headgroups of a DMPC bilayer and (ii) in a TM orientation, in which the principal axis of the α-helix was perpendicular to the bilayer plane. As expected given its *in vivo* environment of the ER/GA membranes, the secondary structure of the model was more stable near a phospholipid bilayer compared to in just a water/ion environment. When initially positioned in the aqueous phase just above the lipid headgroups, the FK1TMD retained its α-helical structure in two short regions at either end of the peptide (Figure 1). The region between these two α-helices (L13 to F20) became unstructured (See supplementary Figure 3). When manually positioned perpendicular to the bilayer plane, the helix generally remained in a stable α-helical conformation (between R3 and H30), although some unfolding was observed at the C-terminal end (Y31 to N36) (see Figure 1 and supplementary Figures 4 and 5). To assess the effect of the bilayer thickness on the stability of FK1TMD, the helix was also simulated in a DPPC lipid bilayer. DPPC has longer tails than DMPC, and thus a thicker hydrophobic core region. The pattern of unfolding at the C-terminal end observed in the DMPC simulations was reproduced in the DPPC simulations. Structural drift of the helix was measured by calculating the mean root mean square deviation (RMSD) of the backbone Cα atoms from the starting structure over the last 25 ns of each simulation. The RMSD values were similar in both lipid environments; 0.33nm ± 0.04, in DMPC compared to 0.28nm ± 0.02 in DPPC (See supplementary Figure 6).

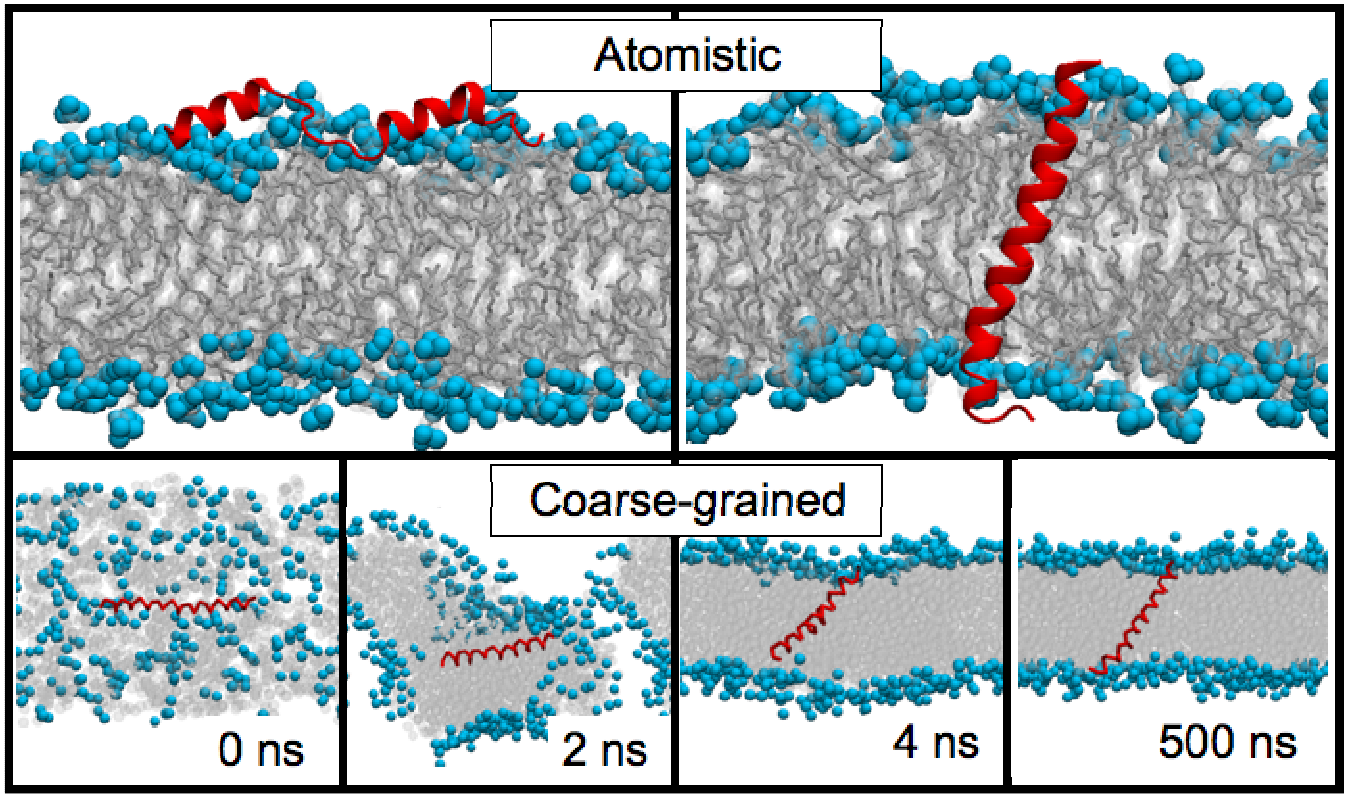

Figure 1. Final snapshots from ATMD after 50 ns in DMPC (top) and DPPC bilayer self-assembly and protein insertion from CGMD (bottom). Lipid headgroups are cyan, the tails are grey and the FK1TMD is red. Water and ions are omitted for clarity.

Coarse-grained simulations. CGMD, in which four heavy atoms are replaced with a single, spherical particle, to reduce the complexity of the system enables longer timescales to be studied. This has permitted the study of bilayer self-assembly and the insertion of peptides into lipid bilayers (*29, 30, 41*). The preferred membrane localization and orientation of FK1TMD has been investigated using CGMD. The FK1TMD model was constrained to an idealized α-helix by using an elastic network. The 1μs simulations were initiated from a random arrangement of lipids, peptide, water and counter-ions to allow the self-assembly of the bilayer and unbiased insertion of the protein. The effect of the bilayer thickness on the orientation of FK1TMD was assessed by simulating the model in DLPC (3 particles in both tails), DPPC (4 particles in both tails) and POPC (4 particles in one tail and 5 in one tail) phospholipids. In all the CG simulations, the bilayer self-assembly proceeded via the stalk formation mechanism as previously reported for DPPC lipids from comparable CGMD studies (*28, 29*). The FK1TMD adopted a

TM orientation within the membrane, with the axis of the α-helix orientated approximately perpendicular to the plane of the bilayer (Figure 1). The FK1TMD was occasionally orientated parallel to the plane of the bilayer at the start of the simulations, particularly in DLPC lipids. However, after a short period of time (~75ns), one end of the helix inserted into the bilayer followed by the rest of the helix, such that it was traversing the bilayer. It retained this TM orientation for the remainder of the simulation, although its precise tilt with respect to the bilayer plane was observed to fluctuate. The tilt angle of FK1TMD calculated during the final 100 ns of the CG simulations was 39° ± 11 in DLPC, and 30° ± 9 in DPPC. Presumably the greater average tilt angle in the shorter DLPC lipid tails is a result of matching the hydrophobic region of the protein with the lipid tails. To further investigate the possibility of the lipid tail length influencing the FK1TMD tilt angle, we ran an additional set of CG simulations, this time with POPC phospholipids. PO tails are longer than DP/DL tails (the POPC CG lipid model implemented within MARTINI has 5 particles for the oleoyl tail and 4 particles for the palmitoyl tail, compared to the 4 particles for each palmitoyl tail in DPPC), and also contain an unsaturated bond (oleoyl group), which give the tails a characteristic 'kink'. In agreement with the trend observed in our DPPC/DLPC simulations of a smaller tilt angle in longer lipid tails, the mean tilt angle of FK1TMD calculated during the final 100 ns of the CG simulations was 17.6 ° ± 7 (see supplementary Figure 7).

A conserved N-terminal motif, R/K-x-x-R/K, has been shown to be required for the correct localization of some glycotransferases within the GA (*3*). The R/K-x-x-R/K motif of FK1TMD (R-I-N-K) is located between residues R3 and K6. To investigate the role of this motif in the membrane localization and orientation of FK1TMD we calculated the number of contacts (contact is defined as inter-atomic distance ≤ 6 Å) between the protein and the phospholipid headgroup particles by sampling the last 100 ns of the 1μs CGMD trajectories at 0.4 ns intervals. Full details of the protein-lipid contacts are provided in the supplementary information. In all three lipid bilayers; DLPC, DPPC and POPC, the N-terminal residues between M1 and N7 made regular contacts with the phospholipid headgroup particles. In particular, R3 and K6 had a high propensity to interact with lipid headgroup particles; together they

accounted for > 20% of all headgroup-protein contacts in simulations of all three lipid bilayers (see supplementary Tables 2, 3 and 4). Presumably these charged residues serve to anchor the N-terminal end of the α-helix in the headgroup region of the zwitterionic lipid bilayer.

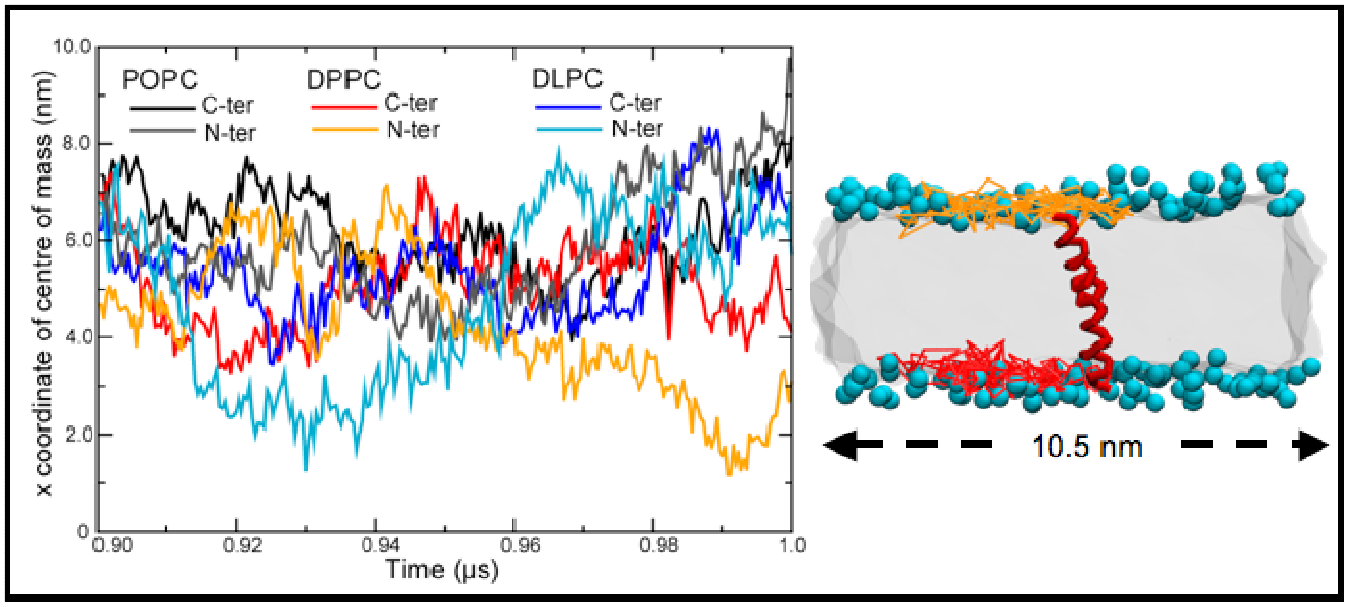

Figure 2. Centre of mass movement of terminal residues of FK1TMD in POPC, DPPC and DLPC lipids (left) and cartoon representation of the same movement in DPPC (right). The bars indicate the maximum and minimum values (x dimension). Lipid phosphate particles are shown in cyan, the tails are represented as a grey surface. The movement of the N-terminal residue is depicted in orange while the C-terminal movement is red.

At the C-terminal end, residues Y28 to N36 made regular contacts with the lipid headgroup particles. In particular, residues K29, R35 and N36 had a marked propensity to interact with the lipid headgroups, together they make up ~15% of the total headgroup-protein contacts in the DLPC simulations and ~20% in the DPPC and POPC simulations. These observations suggest that the charged residues at both N and C-terminal ends of the helix play a key role in anchoring the protein in a TM orientation in the lipid bilayer. The fluctuations in the tilt angles suggest that there may be a degree of mismatch between the width of the hydrophobic patch on FK1TMD and the hydrophobic region of the bilayer defined by the lipid tails. In addition to the protein-lipid contacts, we also measured the protein lateral motion by monitoring the position of the center of mass of the terminal residues in the xy plane during the last 100

ns of the simulations (Figure 2). The helix exhibited a high degree of lateral mobility. In all three lipids, the lateral movement of the helix in the xy plane was of up to ~7 nm in either x or y dimension.

The *in vivo* environment of FK1TMD; the GA membrane is composed of a complex mixture of lipids, including anionic lipid headgroups. Having established the influence of the lipid tail length on FK1TMD orientation and mobility, we then investigated any potential affinity of the protein for particular lipid headgroups, in particular the influence of the anionic lipids. Firstly, we performed self-assembly simulations of the FK1TMD in POPS lipids. Although the high charge density of a 100% POPS bilayer does not reflect the *in vivo* environment of FK1TMD, these simulations were useful to determine the effect of anionic lipid headgroups, as we could compare directly with our simulations of FK1TMD in POPC. The biggest effect of changing the headgroups in our simulations, was on the protein tilt angle. We observed an increase in the tilt angle from 17.6 ° ± 7 in POPC to 25.5 ° ± 9 in POPS. This is presumably driven by the interaction of R3 and K6 in the N-terminus and K29 in the C-terminus with the POPS headgroup atoms (see supplementary Table 5). The lateral mobility of the protein in the two different lipid types was similar. To investigate the effect of the different headgroups in an environment more representative of the GA membrane, we simulated a more complex bilayer. This consisted of a mixture of DPPC, DPPE, PIP2, SM and DPPS lipids in a 50:20:12:10:8 ratio and also cholesterol (CHOL) at a 16:1 phospholipid to cholesterol ratio. (*36*).

In the complex GA membrane, R3 and K6 at the N-terminus of the FK1TMD made a large number of contacts with the headgroups of all lipid types. These two positively charged amino acids made most contacts with the highly negatively charged PIP2. Indeed, the interactions of PIP2 with R3 and K6 accounted for 12% of the total contacts between the FK1TMD and the phospholipid headgroups. In contrast, the interactions of PIP2 with K29 and R35, at the C-terminus of the FK1TMD, only accounted for 5% of the total headgroup contacts. The hydroxyl group of CHOL makes most contacts with a discrete region between I4 and L10 at the N-terminus of the FK1TMD. This region accounted for approximately 55% of the total contacts between CHOL and the FK1TMD. Conversely, CHOL makes fewer and more diffuse contacts with the C-terminal amino acids. The interactions of SM with the

FK1TMD followed the same trends as DPPC. While the tilt angle of the FK1TMD in the more complex GA membrane was 23.6 ± 8; this is intermediate between the tilts observed for the DPPC/DLPC and POPC bilayers, but similar to the tilt angle of 25.5° measured from our simulations of FK1TMD in pure POPS.

To evaluate the distribution of the system components, density profiles of FK1TMD and the various lipid headgroups were calculated (Figure 3). The distribution indicates similar positions of the DPPC, DPPE and DPPS lipids with respect to the bilayer normal, as would be expected for lipids with the same tail groups. The SM lipids are placed slightly further apart, i.e. they are displaced slightly towards the aqueous phase. This appears to be a result of lipid-lipid contacts within the bilayer. The shorter CHOL moieties are located nearer the hydrophobic core of the bilayer. The slight asymmetry in the CHOL density is a result of one molecule flipping into the opposite leaflet during the equilibration procedure. Visual inspection of the simulation trajectories revealed a clustering of PIP2 lipids around the N-terminus of the FK1TMD (Figure 3). To further investigate this clustering, the radial distribution was calculated for the glycerol-linked phosphates of PIP2 relative to the K6 and K29 residues of the FK1TMD (supplementary Figure 8). The distributions show that PIP2 is found more often in a close proximity (within a distance of 1nm) to K6 than to K29. In comparison to PIP2, the radial distribution of the DPPE phosphates was similar in both leaflets of the bilayer. The density of the DPPE phosphates within 1 nm of the FK1TMD was also less than that of PIP2.

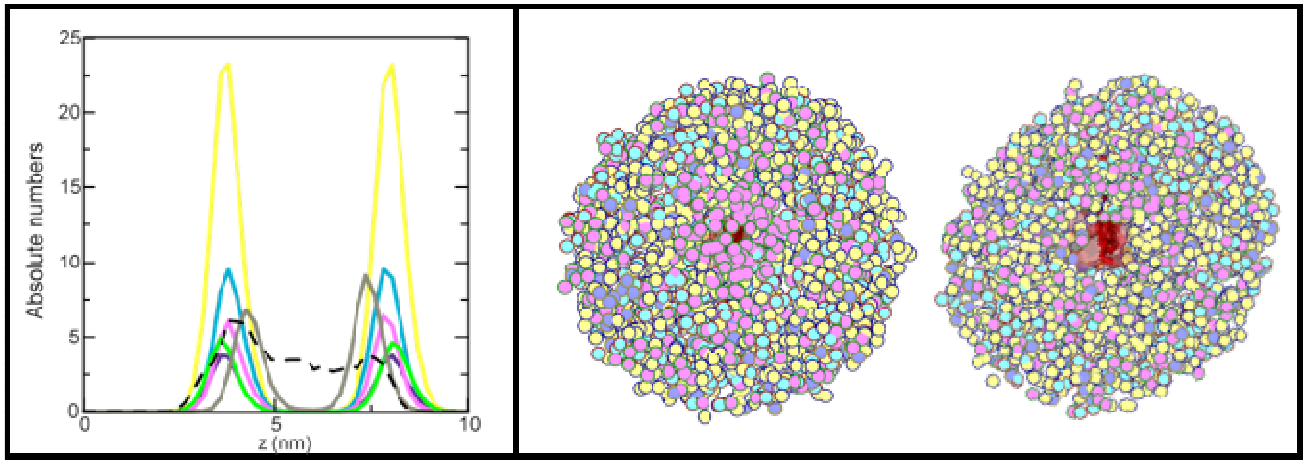

Figure 3. The panel on the left shows the density of protein and lipid headgroup particles along the z dimension. The curves representing the different lipids are coloured as follows: DPPC is yellow, DPPE is cyan, DPPS is violet, PIP2 is magenta, sphingomyelin is green, cholesterol is grey and the black dashed line represents FK1TMD. The panel on the right shows the lipid headgroup particles within 3 nm of the R and K residues in N- (left) and C- (right) termini (colors are as in the left panel, cholesterol and sphingomyelin are omitted for clarity and the FK1TMD is red). The trajectory is fitted on the protein using a least squares procedure and the frames are superimposed at 40 ns intervals over the 1.5 μs trajectory. Clustering of the PIP2 lipids near the N-terminus is evident. Such clustering does not occur in the bilayer leaflet interacting with the C-terminus, which has a more random distribution of lipids.

CD spectroscopy.

The secondary structure of FK1TMD reconstituted into saturated phospholipids of varying chain lengths was investigated using CD spectroscopy. The FK1TMD was reconstituted at a lipid to protein ratio of 100:1 that resulted in the formation of bilayer structures for all lipids with the exception of DHPC where micellar structures are formed. To ensure CD spectra were acquired for all bilayer forming lipids in the liquid crystalline phase data was acquired at both 25°C and 43°C. For all bilayer forming lipids the CD spectra at 25°C and 43°C showed distinct minima at 208 and 222 nm with a maxima at 195nm consistent with FK1TMD forming an α-helical structure as predicted (Figure 4). In contrast the spectra

of FK1TMD in DHPC micelles showed a less distinct minima at 208nm and reduced elipticity at 195nm suggesting that additional secondary structures may contribute the CD spectra observed.

The quantitation of CD spectra of integral membrane proteins and peptides remains challenging due to paucity of membrane proteins structures in the basis sets employed during analysis, the scattering observed from the lipid vesicles (*42, 43*) and other environmental factors (*44*). However, they still provide useful insights into changes in secondary structure composition of proteins and peptides within (or associated) with the lipid bilayer. A quantitative analysis of the α-helical contribution to the CD spectra is given in Table 1. As expected the FK1TMD in bilayer forming lipids is almost entirely α-helical. In the case of the DPPC this indicates that the secondary structure of the FK1TMD remained invariant irrespective of whether the surrounding bilayer was in it liquid crystalline or gel phase. Interestingly, the α-helical contribution to the CD spectra in the bilayer forming lipids appears not to vary as a function of bilayer thickness, suggesting that changes in bilayer thickness are accommodated by changes in the orientation of the TMD within the bilayer in agreement with the molecular dynamics studies. The FK1TMD in DHPC micelles also revealed extensive α-helical structures, with over 90% of the residues in a helical conformation at both temperatures. The analysis of FK1TMD in DHPC micelles at 43°C indicated a small drop in helical content compared to that observed at 25°C although the significance, if any, of this observation will require more detailed structural studies.

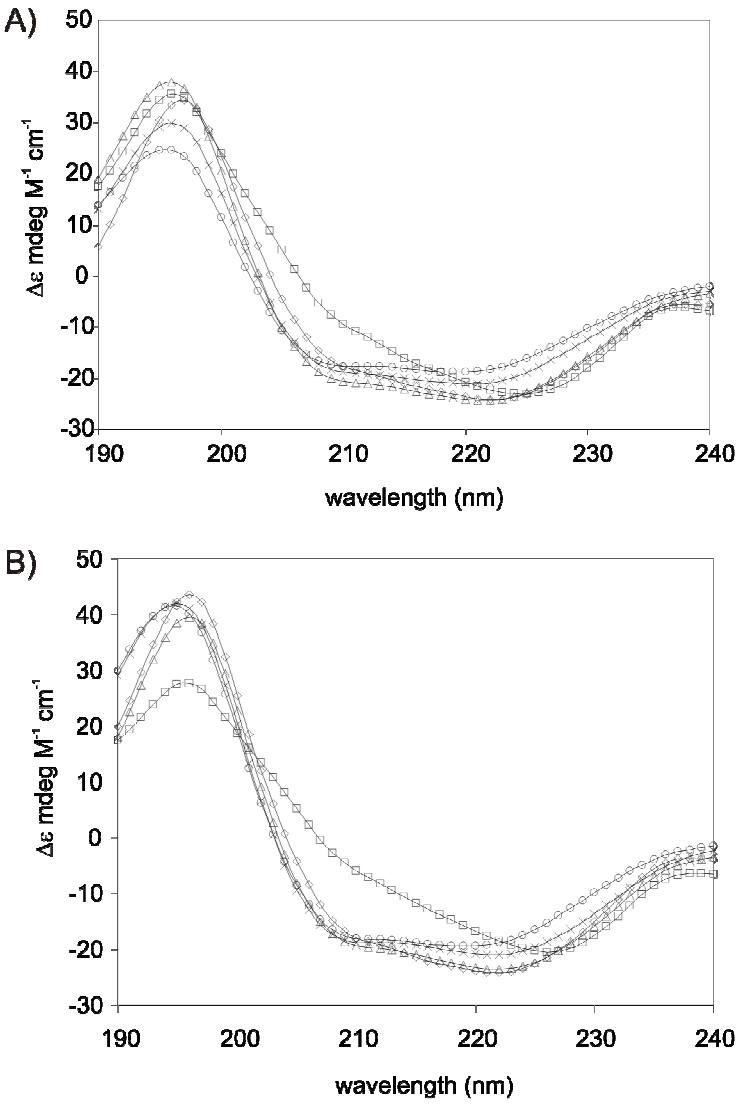

Figure 4. CD spectra of FK1TMD in SUVs of differing lipid chain lengths prepared by sonication at A) 25°C and B) 43°C (C6 (□), C10 (○), C12 (×), C14 (Δ), C16(◊)). The final peptide concentration is 0.2 mg/ml. Each spectrum is an average of 6 acquisitions taken at speed of 100 nm/min. Spectrum displays molar circular dichroism Δε (mdeg M^{-1} cm^{-1}) as a function of wavelength (nm).

Table 1. Alpha helical content of FK1TMD peptide as a function of lipid chain length at 25°C and 43°C. Helical content determined using the CONTIN/LL algorithm (*37, 38*) with basis set 7 within Dichroweb (*39, 40*).

Temperature	

	25°C		43°C	
Chain Length	Helical Content (%)	NRMSD [1]	Helical Content (%)	NRMSD [1]
DHPC	98.7	0.086	90.7	0.120
DDPC	98.2	0.093	97.9	0.078
DLPC	99.6	0.093	99.0	0.068
DMPC	98.8	0.061	98.1	0.054
DPPC	97.4	0.137	97.5	0.069

[1]*The NRMSD (normalized root mean squared deviation) defines the extent of agreement between experimental CD spectrum and that derived during the analysis (2). Note this is not a measure of agreement between the CD spectra and the structures observed in the molecular dynamics simulations.*

DISCUSSION

In conclusion we have used ATMD simulations to assess the stability of FK1TMD. Our simulations have shown that it is a stable α-helix in DPPC and DMPC bilayers in a TM orientation, but partially unfolds when lying parallel to the plain of the bilayer, at the headgroup/water interface. The differences in lipid tail length did not affect the stability of the helix. These results have been corroborated by CD measurements, which confirm that the helical content of the peptide remains invariant as a function of bilayer thickness. CGMD simulations of bilayer self-assembly confirm the preference for the TM orientation. The charged residues anchor both termini of FK1TMD in the headgroup region of the lipid bilayer. To further investigate the effect of lipid tails and headgroups on the membrane orientation and

localization of FK1TMD, we performed CGMD simulations in three different tail lipid tails and also a mixture of headgroups that closely mimics the *in vivo* Golgi membrane composition. To the best of our knowledge, these are the most detailed CGMD simulations of the Golgi membrane, reported to date. Our simulations predict the FK1TMD tilt angle to be sensitive to the composition of the surrounding lipid bilayer. Furthermore, we show that the N-terminus domain of the protein exhibits a marked propensity to interact with PIP2 lipids and may play a role in the formation of microdomains by inducing clustering of these lipids. A possible limitation of this study is that only the TM domain of the fukutin protein is considered, while we note that similar studies of isolated TM domains have previously been used to explore their membrane interactions, the inclusion of neighboring domains would provide additional insights into the dynamics of the functional protein. (*30, 41*)

In summary, our results provide evidence that the TM domain of fukutin is a stable helix, whose stability is not affected by the width of the local membrane. Rather, the protein responds to changes in bilayer thickness by substantial mobility and ability to tilt within the bilayer. The changes observed in the tilt of the helix as a function of bilayer thickness have implications on how the protein may respond to the differing bilayer compositions found within the different intracellular compartments, with implications for protein packing and the formation of higher oligomeric structures as well as its preference for proteins to associate with lipid bilayers with distinct physical properties. These properties are the subject on ongoing investigations with the view to discerning the involvement in the retention of Fukutin and other ER/Golgi resident proteins. Finally, whilst some aspects of the Golgi membrane such as the full extent of lipid tail composition have not been explored in the present study, our simulations of the complex Golgi membrane represent a key step towards linking *in silico* experiments with real biological systems.

ACKNOWLEDGMENT

SK, DAH and TJP thank Phillip Stansfeld and Peter Tieleman for help with lipid parameters.

Supporting Information Available: Detailed description of the material and methods. Analysis: RMSD, secondary structure analysis, protein-lipid contacts and radial distribution functions from simulations. This material is available free of charge via the Internet at http://pubs.acs.org

REFERENCES

1. Martin-Rendon, E., and Blake, D. J. (2003) Protein glycosylation in disease: new insights into the congenital muscular dystrophies, *Trends Pharmacol Sci 24*, 178-183.

2. Torelli, S., Brown, S. C., Brockington, M., Dolatshad, N. F., Jimenez, C., Skordis, L., Feng, L. H., Merlini, L., Jones, D. H., Romero, N., Wewer, U., Voit, T., Sewry, C. A., Noguchi, S., Nishino, I., and Muntoni, F. (2005) Sub-cellular localisation of fukutin related protein in different cell lines and in the muscle patients with MDC1C and LGMD2I, *Neuromusc. Disord. 15*, 836-843.

3. Keramaris-Vrantsis, E., Lu, P. J., Doran, T., Zillmer, A., Ashar, J., Esapa, C. T., Benson, M. A., Blake, D. J., Rosenfeld, J., and Lu, Q. L. (2007) Fukutin-related protein localizes to the Golgi apparatus and mutations lead to mislocalization in muscle in vivo, *Muscle Nerve 36*, 455-465.

4. Matsumoto, H., Noguchi, S., Sugie, K., Ogawa, M., Murayama, K., Hayashi, Y. K., and Nishino, I. (2004) Subcellular localization of fukutin and fukutin-related protein in muscle cells, *J Biochem 135*, 709-712.

5. Lommel, M., Willer, T., and Strahl, S. (2008) POMT2, a key enzyme in Walker-Warburg syndrome: somatic sPOMT2, but not testis specific POMT2, is crucial for mannosyltransferase activity in vivo., *Glycobiology 18*, 615-625.

6. Opat, A. S., van Vliet, C., and Gleeson, P. A. (2001) Trafficking and localisation of resident Golgi glycosylation enzymes, *Biochimie 83*, 763-773.

7. Gleeson, P. A. (1998) Targeting of proteins to the Golgi apparatus, *Histochem Cell Biol 109*, 517-532.

8. Pelham, H. R. B., and Munro, S. (1993) Sorting of membrane proteins in the secretory pathway, *Cell 75*, 603-605.

9. Esapa, C. T., McIlhinney, R. A., and Blake, D. J. (2005) Fukutin-related protein mutations that cause congenital muscular dystrophy result in ER-retention of the mutant protein in cultured cells, *Hum Mol Genet 14*, 295-305.

10. Munro, S. (1998) Localization of proteins to the Golgi apparatus, *Trends in Cell Biology 8*, 11-15.

11. Rayner, J. C., and Pelham, H. R. B. (1997) Transmembrane domain-dependent sorting of proteins to the ER and plasma membrane in yeast, *Embo J. 16*, 1832-1841.

12. Marius, P., Wright, J. N., Findlow, I. S., and Williamson, P. T. (2010) Expression and purification of the transmembrane domain of Fukutin-I for biophysical studies, *Protein Expr Purif 72*, 107-112.

13. Marti-Renom, M. A., Stuart, A. C., Fiser, A., Sanchez, R., Melo, F., and Sali, A. (2000) Comparative protein structure modeling of genes and genomes, *Annu Rev Biophys Biomol Struct 29*, 291-325.

14. Laskowski, R. A., Moss, D. S., and Thornton, J. M. (1993) Main-chain bond lengths and bond angles in protein structures, *J Mol Biol 231*, 1049-1067.

15. Van der Spoel, D., Lindahl, E., Hess, B., Groenhof, G., Mark, A. E., and Berendsen, H. J. C. (2005) Gromacs: Fast, Flexible, and Free, *J Comput Chem 26*, 1701-1718.

16. Berendsen, H. J. C., Vanderspoel, D., and Vandrunen, R. (1995) Gromacs - a Message-Passing Parallel Molecular-Dynamics Implementation, *Comput Phys Commun 91*, 43-56.

17. Hess, B., Kutzner, C., van der Spoel, D., and Lindahl, E. (2008) GROMACS 4: Algorithms for highly efficient, load-balanced, and scalable molecular simulation, *J Chem Theory Comput 4*, 435-447.

18. Schuler, L. D., Daura, X., and Van Gunsteren, W. F. (2001) An improved GROMOS96 force field for aliphatic hydrocarbons in the condensed phase, *J Comput Chem 22*, 1205-1218.

19. Berger, O., Edholm, O., and Jahnig, F. (1997) Molecular dynamics simulations of a fluid bilayer of dipalmitoylphosphatidylcholine at full hydration, constant pressure, and constant temperature, *Biophysical Journal 72*, 2002-2013.

20. Berendsen, H. J. C., Postma, J. P. M., van Gunsteren, W. F., and Hermans, J. (1981) *In Intermolecular Forces*, Reidel, Ed., Dordrecht, The Netherlands.

21. Hess, B. (2008) P-LINCS: A parallel linear constraint solver for molecular simulation, *J Chem Theory Comput 4*, 116-122.

22. Miyamoto, S., and Kollman, P. A. (1992) Settle - an Analytical Version of the Shake and Rattle Algorithm for Rigid Water Models, *J Comput Chem 13*, 952-962.

23. Bussi, G., Donadio, D., and Parrinello, M. (2007) Canonical sampling through velocity rescaling, *J Chem Phys 126*, -.

24. Berendsen, H. J. C., Postma, J. P. M., Vangunsteren, W. F., Dinola, A., and Haak, J. R. (1984) Molecular-Dynamics with Coupling to an External Bath, *J Chem Phys 81*, 3684-3690.

25. Essmann, U., Perera, L., Berkowitz, M. L., Darden, T., Lee, H., and Pedersen, L. G. (1995) A Smooth Particle Mesh Ewald Method, *J Chem Phys 103*, 8577-8593.

26. Kabsch, W., and Sander, C. (1983) Dictionary of Protein Secondary Structure - Pattern-Recognition of Hydrogen-Bonded and Geometrical Features, *Biopolymers 22*, 2577-2637.

27. Humphrey, W., Dalke, A., and Schulten, K. (1996) VMD: Visual molecular dynamics, *J Mol Graphics 14*, 33-&.

28. Marrink, S. J., de Vries, A. H., and Mark, A. E. (2004) Coarse grained model for semiquantitative lipid simulations, *J Phys Chem B 108*, 750-760.

29. Bond, P. J., and Sansom, M. S. (2006) Insertion and assembly of membrane proteins via simulation, *J Am Chem Soc 128*, 2697-2704.

30. Carpenter, T., Bond, P. J., Khalid, S., and Sansom, M. S. P. (2008) Self-assembly of a simple membrane protein: Coarse-grained molecular dynamics simulations of the influenza M2 channel, *Biophysical Journal 95*, 3790-3801.

31. Lopez, C. A., Rzepiela, A. J., de Vries, A. H., Dijkhuizen, L., Hunenberger, P. H., and Marrink, S. J. (2009) Martini Coarse-Grained Force Field: Extension to Carbohydrates, *J Chem Theory Comput 5*, 3195-3210.

32. Lins, R. D., and Hunenberger, P. H. (2005) A new GROMOS force field for hexopyranose-based carbohydrates, *J Comput Chem 26*, 1400-1412.

33. Bond, P. J., Holyoake, J., Ivetac, A., Khalid, S., and Sansom, M. S. (2007) Coarse-grained molecular dynamics simulations of membrane proteins and peptides, *J Struct Biol 157*, 593-605.

34. Bond, P. J., Wee, C. L., and Sansom, M. S. P. (2008) Coarse-Grained Molecular Dynamics Simulations of the Energetics of Helix Insertion into a Lipid Bilayer, *Biochemistry-Us 47*, 11321-11331.

35. Marrink, S. J., Risselada, H. J., Yefimov, S., Tieleman, D. P., and de Vries, A. H. (2007) The MARTINI force field: coarse grained model for biomolecular simulations, *J Phys Chem B 111*, 7812-7824.

36. van Meer, G. (1998) Lipids of the Golgi membrane, *Trends Cell Biol 8*, 29-33.

37. Provencher, S. W., and Glockner, J. (1981) Estimation of globular protein secondary structure from circular dichroism, *Biochemistry 20*, 33-37.

38. van Stokkum, I. H., Spoelder, H. J., Bloemendal, M., van Grondelle, R., and Groen, F. C. (1990) Estimation of protein secondary structure and error analysis from circular dichroism spectra, *Anal Biochem 191*, 110-118.

39. Whitmore, L., and Wallace, B. A. (2004) DICHROWEB, an online server for protein secondary structure analyses from circular dichroism spectroscopic data, *Nucleic Acids Res 32*, W668-673.

40. Whitmore, L., and Wallace, B. A. (2008) Protein secondary structure analyses from circular dichroism spectroscopy: methods and reference databases, *Biopolymers 89*, 392-400.

41. Rouse, S. L., Carpenter, T., Stansfeld, P. J., and Sansom, M. S. P. (2009) Simulations of the BM2 Proton Channel Transmembrane Domain from Influenza Virus B, *Biochemistry-Us 48*, 9949-9951.

42. Wallace, B. A., and Mao, D. (1984) Circular dichroism analyses of membrane proteins: an examination of differential light scattering and absorption flattening effects in large membrane vesicles and membrane sheets, *Anal Biochem 142*, 317-328.

43. Mao, D., and Wallace, B. A. (1984) Differential light scattering and absorption flattening optical effects are minimal in the circular dichroism spectra of small unilamellar vesicles, *Biochemistry 23*, 2667-2673.

44. Swords, N. A., and Wallace, B. A. (1993) Circular-dichroism analyses of membrane proteins: examination of environmental effects on bacteriorhodopsin spectra, *Biochem J 289 (Pt 1)*, 215-219.

Insert Table of Contents artwork here